

Atomic layer deposition of ultrathin blocking layer for low-temperature solid oxide fuel cell on nanoporous substrate

Wonjong Yu, Sanghoon Ji, Gu Young Cho, Seungtak Noh, Waqas Hassan Tanveer, Jihwan An, and Suk Won Cha

Citation: *Journal of Vacuum Science & Technology A* **33**, 01A145 (2015); doi: 10.1116/1.4904206

View online: <http://dx.doi.org/10.1116/1.4904206>

View Table of Contents: <http://scitation.aip.org/content/avs/journal/jvsta/33/1?ver=pdfcov>

Published by the AVS: Science & Technology of Materials, Interfaces, and Processing

Articles you may be interested in

Performance of solid oxide fuel cells approaching the two-dimensional limit

J. Appl. Phys. **115**, 174307 (2014); 10.1063/1.4874738

Effects of proton-conducting electrolyte microstructure on the performance of electrolyte-supported solid oxide fuel cells

J. Renewable Sustainable Energy **5**, 021412 (2013); 10.1063/1.4798491

Redox instability, mechanical deformation, and heterogeneous damage accumulation in solid oxide fuel cell anodes

J. Appl. Phys. **112**, 036102 (2012); 10.1063/1.4745038

Synthesis and calorimetric studies of oxide multilayer systems: Solid oxide fuel cell cathode and electrolyte materials

J. Vac. Sci. Technol. B **28**, C5A1 (2010); 10.1116/1.3420396

Composite cathode based on yttria stabilized bismuth oxide for low-temperature solid oxide fuel cells

Appl. Phys. Lett. **82**, 901 (2003); 10.1063/1.1542933



Advance your technology or engineering career using the **AVS Career Center**, with **hundreds of exciting jobs** listed each month!

<http://careers.avs.org>



Atomic layer deposition of ultrathin blocking layer for low-temperature solid oxide fuel cell on nanoporous substrate

Wonjong Yu

School of Mechanical and Aerospace Engineering, Seoul National University, San 56-1, Daehak dong, Gwanak-gu, Seoul 151-742, South Korea

Sanghoon Ji

Graduate School of Convergence Science and Technology, Seoul National University, 864-1, Iui-dong, Yeongtong-gu, Suwon 443-270, South Korea

Gu Young Cho, Seungtak Noh, and Waqas Hassan Tanveer

School of Mechanical and Aerospace Engineering, Seoul National University, San 56-1, Daehak dong, Gwanak-gu, Seoul 151-742, South Korea

Jihwan An

Manufacturing Systems and Design Engineering Program, Seoul National University of Science and Technology, 232 Gongneung-ro, Nowon-gu, Seoul 139-743, South Korea

Suk Won Cha^{a)}

School of Mechanical and Aerospace Engineering, Seoul National University, San 56-1, Daehak dong, Gwanak-gu, Seoul 151-742, South Korea

(Received 29 August 2014; accepted 3 December 2014; published 16 December 2014)

An ultrathin yttria-stabilized zirconia (YSZ) blocking layer deposited by atomic layer deposition (ALD) was utilized for improving the performance and reliability of low-temperature solid oxide fuel cells (SOFCs) supported by an anodic aluminum oxide substrate. Physical vapor-deposited YSZ and gadolinia-doped ceria (GDC) electrolyte layers were deposited by a sputtering method. The ultrathin ALD YSZ blocking layer was inserted between the YSZ and GDC sputtered layers. To investigate the effects of an inserted ultrathin ALD blocking layer, SOFCs with and without an ultrathin ALD blocking layer were electrochemically characterized. The open circuit voltage (1.14 V) of the ALD blocking-layered SOFC was visibly higher than that (1.05 V) of the other cell. Furthermore, the ALD blocking layer augmented the power density and improved the reproducibility. © 2014 American Vacuum Society. [<http://dx.doi.org/10.1116/1.4904206>]

I. INTRODUCTION

Compared to conventional solid oxide fuel cells (SOFCs) operated at temperatures above 800 °C, low-temperature SOFCs (LT-SOFCs) exhibiting high performance even at temperatures below 600 °C have been considered promising electricity generating sources. This leads to long-term stability, cost effective materials, and excellent applicability for portable energy devices, compact stack parts for stationary devices, and others.¹ A reduction of operating temperatures in LT-SOFCs to temperatures below 500 °C leads to significant ohmic and kinetic losses, which result in poor overall performance.² High ohmic loss deteriorates ionic conductivity due to insufficient thermodynamical energy for the hopping mechanism of oxygen ions, and reducing the electrolyte thickness compensates for the high ohmic loss.^{1–5} The typical configuration of LT-SOFCs with thin film electrolyte is a free standing membrane-electrode assembly (MEA). In this configuration, nanothin, but dense, deposited electrolytes generated excellent performance of LT-SOFCs.^{6–8} However, such free standing MEAs have limitations with respect to the poor thermomechanical stability of nanothin electrolytes^{6–8} while substrate-supported LT-SOFCs have improved

thermomechanical stability. Among a variety of substrates,^{9–12} porous metal and cermet support substrates have been studied for SOFCs application. Porous metal support has superior mechanical strength to any other support substrates, and anode cermet support typically using mixed ion–electron conductor provide much more reaction sites than other support substrates. Despite these strong points, since metal and cermet supports have corrosion issue at operation temperature of SOFCs and microstructural cracking issue, respectively, other support materials need to be developed. The anodic aluminum oxide (AAO) template has been considered as a promising substrate due to the nanoporous channels that ensure active fuel delivery to the reaction sites (or electrolyte–electrode interfaces) and well-matched thermomechanical properties that provide sufficient mechanical strength to the whole cell. In addition, AAO has no issue such as corrosion, diffusion of metal to cell layer, or microcracking. However, the AAO templates have a high possibility of forming pinholes in the deposited thin film electrolytes due to the template's rough surface. Pinhole formation in thin film electrolytes can cause fuel parasitic issues such as fuel crossover and electrode diffusion, which can lead to an increase in leakage current and a decrease in electrode potential between the anode and cathode, or open circuit voltage (OCV).⁵ Ji *et al.*² demonstrated low OCVs below 0.8 V in 700-nm-thick bilayered electrolyte LT-SOFCs

^{a)}Author to whom correspondence should be addressed; electronic mail: swcha@snu.ac.kr

fabricated by pulsed laser deposition on AAO. Additionally, Ha *et al.*⁵ revealed that 240, 340, and 420-nm-thick yttria-stabilized zirconia (YSZ) electrolyte LT-SOFCs fabricated by sputtering only generate low OCVs below 0.5 V.

Sputtering is one of the most frequently used physical vapor deposition (PVD) methods due to its high deposition rate, high uniformity, and excellent microstructural controllability.¹³ Atoms of sputtered thin film are physically combined on substrates as sputtering target is bombarded with energetic ion. Unfortunately, nanothin electrolytes only fabricated by the PVD method on AAO suffered from pinhole issues, as mentioned previously. To reduce the possibility of pinhole formation, atomic layer deposition (ALD), which has excellent conformal and exceptional uniform coating, was used to clog pinholes that originate from AAO templates.^{2,4,5} ALD is well known as a deposition technique for controlling precise thickness of thin film from nano to angstrom scale. The self-limiting surface reaction of ALD facilitates conformal deposition and high step coverage of thin films.^{14,15} Recently, Kwon *et al.*¹⁶ deposited a 20-nm-thick Al₂O₃ blocking layer by ALD in the middle of PVD electrolyte layers, to show the OCVs of the cells drastically augmented from 0.05 to 1.02 V. Nevertheless, an additional postetching process was necessary for the Al₂O₃ blocking layer, because it can act as an insulating matter for ion conduction through the electrolyte. Therefore, to omit this cumbersome process, ionic conducting materials need to be utilized as ALD blocking layers.

This study investigates the effects of inserting a “conformal and reproducible” ultrathin oxygen ion that conducts ALD blocking layer between two sputtered electrolyte layers in LT-SOFCs, which suppress pinhole formation that originates from AAO template nanopores. For the high efficiency of cost and time, sputter was used with ALD for the fabrication of cells. To verify the effects of inserting an ALD blocking layer, a cell without an ALD blocking layer was comparatively characterized in terms of electrochemical and microstructural property.

II. EXPERIMENT

A. Thin film fabrication

LD YSZ film was fabricated by using a showerhead-type commercial atomic layer deposition system (Atomic Premium, CN1, South Korea). The chamber's base pressure was set to 20 mTorr using a dry pump. The stage temperature was set to 250 °C. Tetrakis(dimethylamido) zirconium, Zr(NMe₂)₄, and Tris(methylcyclopentadienyl) yttrium, Y(MeCp)₃, were used as precursors of zirconia and yttria, respectively. The temperatures of the canisters were 50 and 145 °C, and the temperatures of the lines for zirconia and yttria deposition were 70 and 155 °C, respectively. An electropolished stainless steel bubbler was filled with the precursor and fed 300 sccm Ar gas with 99.99% purity. Zirconia monolayer was synthesized by precursor pulsing for 3 s, purging for 30 s, oxidant pulsing for 1 s, generating plasma for 8 s, and purging for 30 s. Yttria monolayer was synthesized by precursor pulsing for 5 s, purging for 60 s, oxidant pulsing for 1 s, generating plasma for 8 s, and

purging for 60 s. O₂ gas widely utilized to deposit ALD YSZ was used as an oxidant, its volumetric flow was 100 sccm.⁵ Our ALD YSZ film had low carbon-concentration (~1.5%). In YSZ deposition, zirconia was deposited before yttria, and the ratio of zirconia and yttria ALD cycles were set to 7:1. X-ray photoelectron spectroscopy (XPS) analysis showed that the atomic concentrations of the ALD YSZ thin film were Zr 3d = 34.8%, Y 3d = 4.9%, O 1s = 58.8%, the yttria mole fraction of the ALD YSZ was ~7.7 mol. %. The growth rate of ALD YSZ film was ~1.4 Å/cycle.

PVD films were deposited by a commercial sputtering machine (A-Tech System Ltd, Korea) equipped with a rotating unit. All PVD films were deposited at a rotation rate of 4 rpm to reduce the variations in growth rate. The target to substrate distance was fixed to 80 mm and a YSZ (Y_{0.16}Zr_{0.84}) metal target was used to deposit PVD YSZ films. PVD YSZ films with dense microstructure were deposited under 5 mTorr Ar atmosphere with a purity of 99.9999%. A direct current power source set to 100 W was used and the PVD YSZ film depositing rate was ~200 nm/h. Dense PVD gadolinium-doped ceria (GDC) (Gd_{0.1}Ce_{0.9}O_{1.95}) films were deposited under 10 mTorr Ar/O₂ atmosphere. The radio frequency (RF) power source was set to 50 W and the PVD GDC film depositing rate was ~40 nm/h. Platinum (Pt) films were deposited by RF sputtering in Ar atmosphere. Dense Pt anode was deposited at 5 mTorr with 200 W power at a deposition rate of ~40 nm/min. Porous Pt cathode was deposited at 50 mTorr with 50 W with a deposition rate almost identical to that for dense Pt anode.

B. Thin film characterization

XPS (AXIS, Kratos Analytical, Japan) was used to investigate the composition of the sample surfaces. Before the analysis, the surface of the sample was etched by 1 keV Ar ion with 1 μA current for 10 s to eliminate the possibility of contamination. A focused ion beam and field emission scanning electron microscopy (FIB/FE-SEM) (3D FEG, FEI Company, Netherland) was used to verify the layer structures and surface microstructure of the samples. Each sample was coated with Pt to prevent surface etching by the focused ion beam.

C. Electrochemical characterization

Electrochemical evaluation was conducted using a customized SOFC station with a micro probing setup. For electrochemical measurements, the anode side was attached using a commercial sealant (CP4010, Aremco Products, Inc., USA) and Ag paste (597A, Aremco Products, Inc., USA) while the cathode side used a hardened-steel probe. The furnace was heated up to 500 °C at a ramping rate of 10 °C/min. During the test, dry H₂ was supplied to the anode with a flow rate of 50 sccm while the cathode side was exposed to atmospheric air. Electrochemical characterization was carried out by a commercial electrochemical test system (1287/1260, Solatron Analytical, UK).

III. RESULTS AND DISCUSSION

A. Configuration of ALD YSZ blocking-layered cell

GDC is in the limelight among SOFC electrolytes due to its relatively high ionic conductivity and surface exchange coefficient.¹⁷ However, GDC is reduced at low oxygen partial pressure conditions and becomes electrically conductive, which lowers OCV.¹⁸ Even though reduction phenomena of GDC is not greatly affecting the potential of fuel cell at below 500 °C, our group confirmed that OCV of GDC electrolyte cell was low as 0.9 V even at below 500 °C, which suggest that GDC could be reduced at low temperature.² For this reason, GDC is often used with zirconia-based blocking layers with higher stability at reduction atmosphere,^{19,20} which is why YSZ was used as material for the blocking layer in this study. The thickness of PVD electrolyte layers was arbitrarily selected to examine the effects of pinholes that originate from AAO pores. Most of the LT-SOFCs in porous supports use $\sim 1 \mu\text{m}$ or thicker electrolytes to prevent pinhole formation in thin film electrolytes.²¹ In this study, the relatively thin electrolyte was utilized to clarify the effects of a conformal blocking layer inhibiting pinholes formation. Kwon *et al.*¹⁶ showed that columns growing on AAO surface gradually merged as the thickness of the columns themselves increased, and pinholes were extended to 500 nm from the AAO surface. If the PVD electrolyte is too thick, pinholes-related effects on the electrode potential are nondetectable. Therefore, the 300-nm-thick PVD electrolyte cell will be influenced by pinholes in terms of electrochemical performance.

Figure 1 is a schematic of the depositing ALD YSZ blocking layer and electrochemical test system as well as a cross-sectional view of the cell with ALD YSZ blocking layer. The ALD YSZ blocking layer deposited during 200 cycles was inserted between a 200-nm-thick PVD YSZ and a 100-nm-thick PVD GDC. Figure 1(c) shows a FE-SEM cross-sectional image for the cell with an ALD YSZ blocking layer (hereafter called the ALD-blocked cell), which is comprised of a trilayer electrolyte (bottom PVD YSZ, ALD YSZ, and PVD GDC) and two Pt electrodes. The fabrication process of a cell without an ALD YSZ blocking layer (hereafter called the PVD cell) is identical to that of the ALD YSZ blocking-layered cell, except without ALD YSZ deposition. A few nanometer-thick ALD YSZ blocking layers were considered adequate for pinhole blockage,¹⁶ but a 30-nm-thick ALD layer was deposited to reliably block the pinholes in the PVD YSZ. Test cells were fabricated on 80 nm pore-sized AAO substrates. 300-nm-thick dense Pt was used as electrode-catalysts on the anode side while 250-nm-thick porous Pt was used as electrode-catalysts on the cathode side and its area was 1 mm^2 .

B. Insertion effects of the ALD pinhole blocking layer

The electrochemical performance of ALD-blocked and PVD cells was evaluated to verify the effects of inserting the ALD blocking layer. The insertion of the blocking layer was expected to increase OCV as the ALD layer suppressing pinhole because the blocking layer hinders the fuel crossover through pinholes. Figure 2 shows the OCV and normalized overpotential of ALD-blocked and PVD cells for 2 h.

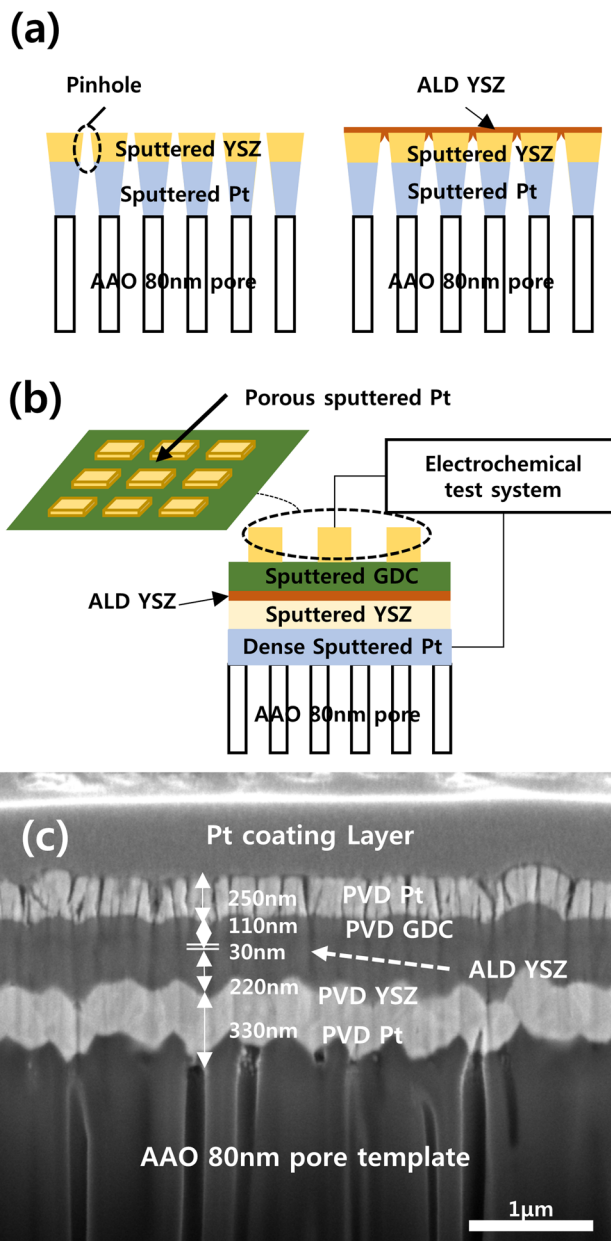


Fig. 1. (Color online) (a) Schematic of ALD blocking layer, (b) schematic of electrochemical test system explained with overall layers. (c) Cross-sectional view of cell with ALD blocking layer from FE-SEM.

Figure 2(a) shows the number of electrodes that properly operate over 2 h at 500 °C, which validates the reproducibility of electrolytes under the presumption that it has been reported that thin film electrolyte having poor uniformity can easily suffer from pinhole issue, followed by short circuit phenomena or fast degradation will appear immediately.²² Initial OCVs for nine cells were normally measured at both ALD-blocked and PVD cells. One hour after the initial operation, PVD cells showed 66% survival rate compared to ALD-blocked cells with 100%. After 2 h, ALD-blocked cells still showed a survival rate of 100%, while that of PVD cells reached zero due to electrical shortage in all cells. Thus, ALD-blocked cells are less affected by pinholes that lead to short circuiting or fast degradation and have higher reproducibility.

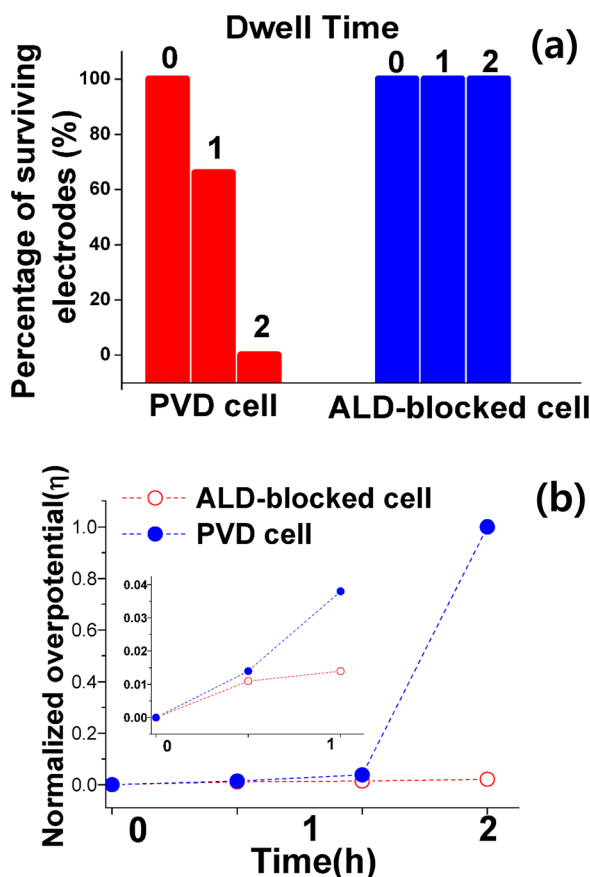


Fig. 2. (Color online) (a) Percentage of survival electrodes for both ALD-blocked (with electrolyte deposited by combination of PVD and ALD) and PVD cells (with electrolyte deposited by PVD only), and (b) normalized overpotential for both ALD-blocked and PVD cells.

Figure 2(b) shows the time behavior of normalized overpotential for ALD-blocked and PVD cells and the initial OCV for the two cells was 1.14 and 1.05 V, respectively. The OCV difference was initially slight above 0.1 V. The difference grew gradually for about 80 min, and after that it was drastically increased due to a sharp decrease in OCV of PVD cell. This difference is minor at the beginning of measurement, but for long-term operation, the difference could be considered as an indicator representing durability of the cell's performance. Furthermore, this OCV difference can show that an ALD blocking layer successfully clog pinholes in PVD YSZ electrolyte. The possible reason for the higher degradation rate of PVD cells is the annealing effect of PVD electrolyte layers. The binding force of physically deposited films is weaker than that of chemically deposited films.²³ Although the PVD electrolyte layers used in this study were deposited at room temperature, the cells were electrochemically measured at 500 °C.²⁴ Therefore, the PVD electrolyte layers will most likely be readily deformed and then degrade cell performance.

C. Electrochemical characterization of the cell with and without ALD blocking layer

The pinholes through the PVD electrolyte layers can be blocked by uniform and conformal deposition of an ultrathin

ALD blocking layer. Figure 3 shows the power density versus current density for the ALD-blocked and PVD cells. As clearly shown, the peak power density of the ALD-blocked cell (172 mW/cm²) was ~20% higher than that of the PVD cell (146 mW/cm²). To examine electrochemical properties of each cells, electrochemical impedance spectroscopy (EIS) analysis was conducted for ALD-blocked and PVD cells, which is presented in Fig. 4. EIS data of cells with ALD were measured from high frequency (2 MHz) to low frequency (2 Hz) at 0.5 V and OCV bias, respectively. In EIS analysis, the high-frequency intersecting point between the EIS curve and real (X) axis indicates ohmic resistance, including current collecting and ionic resistance.²⁵ The little difference in ohmic resistance for two cells (0.03 Ω cm²) indicates no significant changes in ohmic resistance due to ALD blocking layer insertion. In addition, to investigate the effects of electrolyte grain boundary through EIS data, the semicircles at two different bias voltages were comparatively characterized as shown in Fig. 4(a). Shim *et al.* recently reported that the semicircles in EIS curves at high frequencies range are related to grain boundary effect of electrolyte.²⁶ From this report, we can speculate that the shape of semicircles that correspond to electrolyte grain boundaries do not change with the change of bias voltage.^{3,25,26} In Fig. 4(a), EIS curves in two cells did not overlap at high frequencies range, which indicates that cell resistance related to electrolyte grain boundary is negligible.^{25,26} Figure 4(b) shows the EIS data measured under a bias voltage of 0.5 V. On a closer view, there are two semicircles presenting an appearance of overlapped two semicircles and a bigger semicircle at lower frequencies is regarded as interfacial resistance at the cathode side.²⁵ This is because the cathode in LT-SOFCs generally has significantly low reaction kinetics compared to the anode, which result in appearing as larger semicircle in EIS data.^{16,27} As shown in this figure, the first semicircles of both cells are similar, but the second semicircle's radius of the ALD-blocked cell is 0.5 Ω cm² smaller than that of the PVD cell. This means that the performance difference between the two kinds of cells resulted from cathode charge-transfer resistance differences. Therefore, activation loss in the cathode

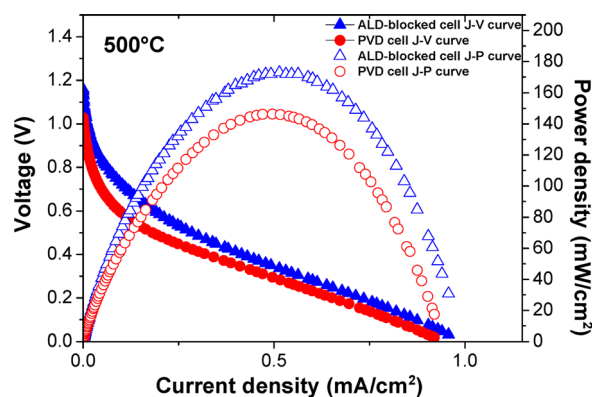


Fig. 3. (Color online) Power density and voltage vs current density curves of ALD-blocked and PVD cells.

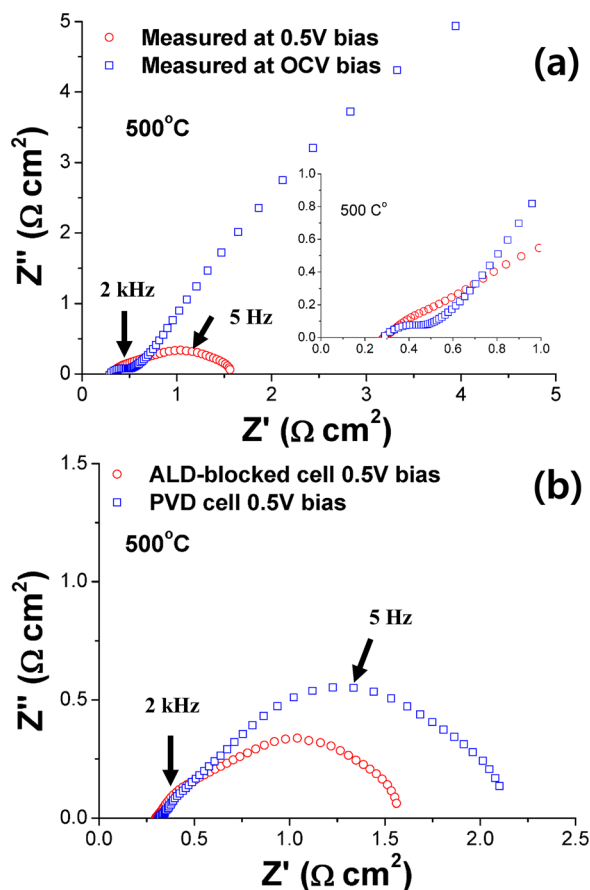


FIG. 4. (Color online) (a) Voltage bias study for an ALD-blocked cell. (b) Impedance comparison of ALD-blocked and PVD cells.

side is thought to be the dominant factor affecting the performance.

The reason of the difference of activation loss for both cells is the different electrode surface morphology on the cathode side. Since the cells were deposited by layer upon layer, surface morphology of ALD electrolyte should affect the characteristics of the electrolyte–electrode interface. Thus, by investigating the surface of the electrolyte, surface characteristics of ALD and the interface between the electrolyte and electrode layers could be characterized. The electrochemical performance at the electrolyte–electrode interface is under the control of a number of reaction sites, which is usually known as triple phase boundaries (TPBs)²⁸ where the electrode, electrolyte, and reactant meet. The characterization related to TPB length is necessary to describe the performance difference. As shown in Figs. 5(a) and 5(b), even though atomic force microscopy (AFM) analysis did not show significant difference of the root mean square roughness (Rq) representing the uniformity of surface, the electrode surface of the ALD-blocked cell had smaller grain size than the PVD cell. In Figs. 5(c) and 5(d), line profile of AFM was done for both cells. This analysis may not be precise measurement for average grain size of the thin films. However, we can speculate the difference of grain size from this. In Figs. 5(a) and 5(b), grain size of ALD-blocked cells can be considered as ~ 250 nm and that of PVD cells is ~ 350 nm. The difference is around 100 nm. The smaller size of the grain might be originated from ALD blocking layer having much fine grain size than PVD layer. It is well known that the reaction rate of oxygen dissipation is much faster at grain boundaries than bulk surfaces.²⁶ Thus, the smaller

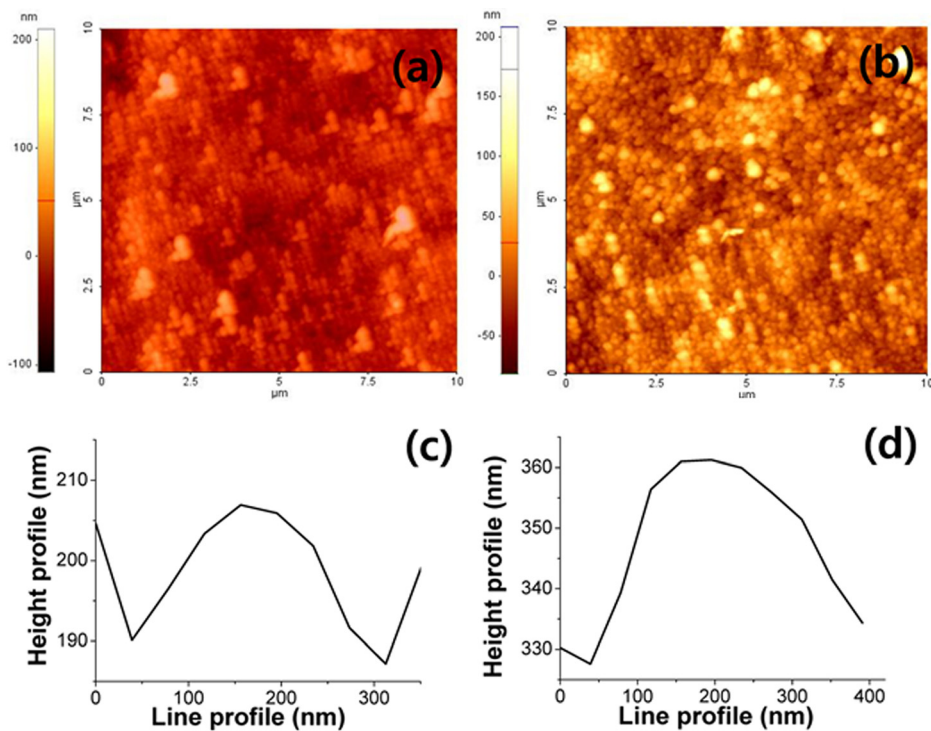


FIG. 5. (Color online) AFM analysis on the surfaces of (a) ALD-blocked and (b) PVD cells. Line profile from AFM data for both (c) ALD-blocked and (d) PVD cells.

grain sizes of the electrolyte–electrode interface for ALD-blocked cell provide more grain boundaries considered as longer TPBs that lead to faster reaction kinetics at the cathode side.^{29,30} Future works will include different kinds of characterization to obtain more accurate information about interfacial reactions.

IV. SUMMARY AND CONCLUSIONS

We successfully applied a ~30-nm-thick ultrathin ALD blocking layer to nanoporous substrate-supported LT-SOFC. The pinholes formed at PVD electrolyte layers could be blocked by the ALD blocking layer. The ALD-blocked PVD electrolyte cell showed higher OCV and more excellent reliability for long term operation, compared to the PVD electrolyte cell. In addition, the ALD-blocked PVD electrolyte cell generated higher peak power density than the PVD electrolyte cell due to the faster reaction kinetics on the cathode side by smaller grain size. Consequently, this study presents that ultrathin ALD layers can be utilized for fabrication of thin film electrolytes to improve microstructural stability and electrochemical performance. We believe that the work presented here may have implications in realizing the high power LT-SOFCs with large active area based on porous substrates.

ACKNOWLEDGMENTS

This work was supported by the New & Renewable Energy Development Program of the Korea Institute of Energy Technology Evaluation and Planning (KETEP) grant funded by the Korea government Ministry of Knowledge Economy (No. 20113020030010).

¹A. B. Stambouli and E. Traversa, *Renew. Sustainable Energy Rev.* **6**, 433 (2002).

²S. Ji, I. Chang, Y. H. Lee, J. Park, J. Y. Paek, M. H. Lee, and S. W. Cha, *Nanoscale Res. Lett.* **8**, 48 (2013).

³R. O'Hayre, S. W. Cha, W. Colell, and F. B. Prinz, *Fuel Cell Fundamentals* (John Wiley & Sons, New York, 2009).

⁴C. Bernay, A. Ringuedé, P. Colombari, D. Lincot, and M. Cassir, *J. Phys. Chem. Solids* **64**, 1761 (2003).

⁵S. Ha, P.-C. Su, and S.-W. Cha, *J. Mater. Chem. A* **1**, 9645 (2013).

⁶J. H. Shim, C.-C. Chao, H. Huang, and F. B. Prinz, *Chem. Mater.* **19**, 3850 (2007).

⁷P.-C. Su, C.-C. Chao, J. H. Shim, R. Fasching, and F. B. Prinz, *Nano Lett.* **8**, 2289 (2008).

⁸H. Huang, M. Nakamura, P. C. Su, R. Fasching, Y. Saito, and F. B. Prinz, *J. Electrochem. Soc.* **154**, B20 (2007).

⁹H.-S. Noh, H. Lee, B.-K. Kim, H.-W. Lee, J.-H. Lee, and J.-W. Son, *J. Power Sources* **196**, 7169 (2011).

¹⁰S. D. Kim, S. H. Hyun, J. Moon, J.-H. Kim, and R. H. Song, *J. Power Sources* **139**, 67 (2005).

¹¹J.-H. Koh, Y.-S. Yoo, J.-W. Park, and H. C. Lim, *Solid State Ionics* **149**, 157 (2002).

¹²M. C. Tucker, G. Y. Lau, C. P. Jacobson, L. C. DeJonghe, and S. J. Visco, *J. Power Sources* **175**, 447 (2008).

¹³W. Liu, B. Li, H. Liu, and W. Pan, *Electrochim. Acta* **56**, 8329 (2011).

¹⁴S. M. George, *Chem. Rev.* **110**, 111 (2010).

¹⁵M. Cassir, A. Ringuedé, and L. Niinistö, *J. Mater. Chem.* **20**, 8987 (2010).

¹⁶C.-W. Kwon, J.-W. Son, J.-H. Lee, H.-M. Kim, H.-W. Lee, and K.-B. Kim, *Adv. Funct. Mater.* **21**, 1154 (2011).

¹⁷Y. B. Kim, J. H. Shim, T. M. Gür, and F. B. Prinz, *J. Electrochem. Soc.* **158**, B1453 (2011).

¹⁸B. C. H. Steele, *Solid State Ionics* **129**, 95 (2000).

¹⁹S. Cho, Y. N. Kim, J.-H. Kim, A. Manthiram, and H. Wang, *Electrochim. Acta* **56**, 5472 (2011).

²⁰C. Brahim, A. Ringuedé, E. Gourba, M. Cassir, A. Billard, and P. Briois, *J. Power Sources* **156**, 45 (2006).

²¹D.-H. Myung, J. Hong, K. Yoon, B.-K. Kim, H.-W. Lee, J.-H. Lee, and J.-W. Son, *J. Power Sources* **206**, 91 (2012).

²²A. Evans, A. B.-Hütter, J. L. M. Rupp, and L. J. Gauckler, *J. Power Sources* **194**, 119 (2009).

²³P. C. Jindal, D. T. Quinto, and G. J. Wolfe, *Thin Solid Films* **154**, 361 (1987).

²⁴S. Ji, I. Chang, G. Y. Cho, Y. H. Lee, J. H. Shim, and S. W. Cha, *Int. J. Hydrogen Energy* **39**, 12402 (2014).

²⁵T. Tsai and S. A. Barnett, *J. Vac. Sci. Technol., A* **13**, 1073 (1995).

²⁶J. H. Shim, J. S. Park, T. P. Holme, K. Crabb, W. Lee, Y. B. Kim, X. Tian, T. M. Gür, and F. B. Prinz, *Acta Mater.* **60**, 1 (2012).

²⁷H.-S. Noh, K. J. Yoon, B.-K. Kim, H.-J. Je, H.-W. Lee, J.-H. Lee, and J.-W. Son, *J. Power Sources* **247**, 105 (2014).

²⁸S. W. Cha, R. O'Hayre, and F. B. Prinz, *Solid State Ionics* **175**, 789 (2004).

²⁹E. Mutoro, B. Luerssen, S. Güntherb, and J. Janek, *Solid State Ionics* **179**, 1214 (2008).

³⁰J. H. Shim, J. S. Park, J. An, T. M. Gür, S. Kang, and F. B. Prinz, *Chem. Mater.* **21**, 3290 (2009).